# Sonochemical Synthesis and Characterization of $Ni(C_4H_6N_2)_6(PF_6)_2$, $Fe(C_4H_6N_2)_6(BF_4)_2$, and $Ni(C_4H_6N_2)_6(BF_4)_2$ in 1-Butyl-3-methylimidazole with Hexafluorophosphate and Tetrafluoroborate

**David S. Jacob,[a] Shirli Makhluf,[a] Ishay Brukental,[b] Ronit Lavi,[b] Leonid A. Solovyov,[c] Israel Felner,[d] Israel Nowik,[d] Rachel Persky,[a] Hugo E. Gottlieb,[a] and Aharon Gedanken*[a]**

**Keywords:** Ionic liquids / Sonochemistry / Iron / Nickel / Imidazole / X-ray powder diffraction / Structure analysis

This paper reports on the inorganic sonochemical synthesis of crystalline $Ni(C_4H_6N_2)_6(PF_6)_2$, $Fe(C_4H_6N_2)_6(BF_4)_2$, and $Ni(C_4H_6N_2)_6(BF_4)_2$ in the ionic liquids, 1-butyl-3-methylimidazolium hexafluorophosphate $(BMI)^+(PF_6)^-$ and 1-butyl-3-methylimidazolium tetrafluoroborate $(BMI)^+(BF_4)^-$. The structures of the compounds were determined and refined by using powder X-ray diffraction methods. The salts crystallize in the trigonal $P\bar{3}$ space group. IR, Raman and $^{19}F$ NMR spectroscopic studies confirm that the $PF_6^-$ and $BF_4^-$ anions are not bonded to the metal cations. Magnetic measurements reveal the paramagnetic nature of the complexes. Mössbauer investigations show that the iron atom in $Fe(C_4H_6N_2)_6(BF_4)_2$ is in the oxidation +2 state. The broad EPR signals, which reflect the octahedral symmetry of the nickel complexes, were measured for $Ni(C_4H_6N_2)_6(PF_6)_2$ and $Ni(C_4H_6N_2)_6(BF_4)_2$.


## Introduction

Room-temperature ionic liquids (RTILs) have aroused increasing interest worldwide as solvents, templates, and charge-compensating groups for numerous types of reactions due to their unique physical properties.[1a–1d] There are only very few reports in the area of synthetic coordination chemistry in ionic liquids.[2–5]

Recently, we have presented a report on the inorganic sonochemical synthesis of a $Fe^{II}(1\text{-methylimidazole})_6(PF_6)_2$ in $(BMI)^+(PF_6)^-$ ionic liquid solvents.[6] The product was obtained as a result of the sonochemical decomposition of $Fe(CO)_5$ in $(BMI)^+(PF_6)^-$. The charge on the $Fe^{II}$ ion in the complex is stabilized by the two $PF_6^-$ anions originating from the ionic liquid. We found that the $PF_6^-$ anions enter the final structure, wherein the ionic liquids act as clean and effective solvents for the crystallization of the complex. However, it is usually assumed that the ionic liquids are entirely innocuous and noncoordinating solvents.

[a] Department of Chemistry and Kanbar Laboratory for Nanomaterials at the Bar-Ilan University Center for Advanced Materials and Nanotechnology, Bar-Ilan University, 52900 Ramat-Gan, Israel
E-mail: gedanken@mail.biu.ac.il
[b] Department of Physics, Bar-Ilan University, 52900 Ramat-Gan, Israel
[c] Institute of Chemistry and Chemical Technology, Siberian Branch, Russian Academy of Sciences, 660049 Krasnoyarsk, Russia
[d] The Racah Institute of Physics, The Hebrew University of Jerusalem, 91904 Jerusalem, Israel

In the current study, we have continued to explore inorganic sonochemical reactions in ionic liquids, and in this paper, we report the synthesis of iron and nickel complexes of 1-methylimidazole in two different ionic liquids (as solvents) under sonochemical conditions using carbonylmetal compounds as precursors. The precursors in all these cases are the corresponding carbonyl complexes [$Fe(CO)_5$ and $Ni(CO)_4$], which are not soluble in $(BMI^+)(PF_6^-)$ and $(BMI^+)(BF_4^-)$ ionic liquids. It is well known that pentacarbonyliron and tetracarbonylnickel yield amorphous iron and amorphous nickel when sonicated in decalin (or any other nonvolatile organic solvent) under argon.[7a,7b] On the other hand, the decomposition of $Fe(CO)_5$ and $Ni(CO)_4$ in decalin under oxygen yields amorphous metal oxides.[8] The sonochemical decomposition of these carbonyl complexes in $(BMI^+)(PF_6^-)$ and $(BMI^+)(BF_4^-)$ form crystalline products. The current paper demonstrates the generality of our previous study, and that in none of the four cases (two carbonyl complexes in two solvents) are metal oxides formed.

The sonochemical products of the decomposition of the carbonyl complexes in ionic liquids are crystalline. They differ from the amorphous products formed when the same reactions are performed in nonvolatile organic solvents. In the sonochemical reactions in ionic liquids, we found that the anions of the ionic liquid solvents serve as charge-compensating groups and cause the crystallization of the products.

Powder X-ray diffraction (PXRD) is used to investigate the crystal structure of the metal complexes synthesized un-

 **DOI: 10.1002/ejic.200500024**  

der the sonochemical conditions. The synthesized inorganic complexes are characterized by C, H, N analysis and several spectroscopic methods, such as Mössbauer, IR, Raman, MS, EPR, and $^{19}F$ NMR. The thermal stability of the (*N*-methylimidazole)metal complexes and of ionic liquid solvents is studied with the help of thermal gravimetric analysis (TGA). The magnetic properties of the synthesized complexes of iron and nickel are also reported in this paper.

## Results and Discussion

### Powder XRD

The unit cell parameters (Table 1) of (1-methylimidazole)$_6$-Ni$(PF_6)_2$ (**A**), (1-methylimidazole)$_6$Fe$(BF_4)_2$ (**B**) and (1-methylimidazole)$_6$Ni$(BF_4)_2$ (**C**) were determined from PXRD peak positions. The initial atomic coordinates were derived from the structure models of (1-methylimidazole)$_6$-Fe$(PF_6)_2$,[6] (5-methylpyrazole)$_6$Ni$(ClO_4)_2$,[9] and (2-methyltetrazole)$_6$Ni$(BF_4)_2$,[10] whose unit-cell dimensions and PXRD patterns are analogous to those of **A**, **B** and **C**. The crystal structure of **A** was found to be identical to that of (1-methylimidazole)$_6$Fe$(PF_6)_2$.[6] The structure refinement was performed by applying the Derivative Difference Minimization (DDM)[11] method, in which derivatives of the profile difference are minimized, instead of the squared difference, which allows a full-profile refinement independently of the underlying background curve. The calculations were carried out using a computer code package based on a corrected and modified version of the Rietveld[12] refinement program DBWS.[13] The PXRD patterns of both **B** and **C** exhibited very complex background components caused, presumably, by an amorphous admixture and the structural faults discussed below, which made the application of DDM essential.

The PXRD structure refinement and the electron density map analysis of **B** and **C** revealed additional pseudo-positions of metal and fluorine atoms in the unit cell, which are related to the main ones by a mirror plane operation ($x$, $y$, $1/2 - z$). The presence of these positions was indicative of structural faults such as twin and/or line defects. The twinning and molecular disorder is known to be a typical phenomenon for structures of this type.[6,9,10,14a,14b] To allow for the presence of the faults, the structure model of **B** and **C** was constructed from two sub-sets of atomic positions related to each other by the mirror plane. The occupancies of the two sub-sets were refined independently for the anions and the cations applying the stoichiometric constraints. Atomic coordinates of methylimidazole were allowed to refine with soft constraints applied to the C–C and the C–N distances. The hydrogen atoms were added geometrically and refined using the riding model.

The structure refinement results are summarized in Tables 1, 2, 3 and 4. The final consistency between the observed and calculated PXRD profiles after the DDM structure refinement is illustrated in Figure 1. The crystal structure and the alternative positions of molecules in the unit cell are shown in Figures 2 and 3. The metal atoms in **A**, **B** and **C** have a typical octahedral coordination of six equivalent nitrogen atoms of the methylimidazole groups. The tetrafluoroborate anion has two alternative orientations with equal probabilities as follows from the occupancies of the respective atomic positions (Tables 2 and 3). The occupancies of the alternative pseudo-positions related to the (methylimidazole)metal complexes indicate a high concentration of the structural faults. The faults, in turn, may be responsible for the atomic disorder reflected in the high isotropic displacement parameters.

Table 1. Crystallographic details.

| | **A** | **B** | **C** |
|---|---|---|---|
| Empirical formula | $Ni(C_4H_6N_2)_6(PF_6)_2$ | $Fe(C_4H_6N_2)_6(BF_4)_2$ | $Ni(C_4H_6N_2)_6(BF_4)_2$ |
| Formula mass | 841.27 | 722.09 | 724.95 |
| Crystal system | trigonal | trigonal | trigonal |
| Space group | $P\bar{3}$ | $P\bar{3}$ | $P\bar{3}$ |
| $a$ [Å] | 11.3758(2) | 11.2574(5) | 11.1678(3) |
| $c$ [Å] | 7.9948(1) | 7.7756(3) | 7.7560(2) |
| $V$ [Å$^3$] | 895.99(2) | 853.38(6) | 837.73(4) |
| $Z$ | 1 | 1 | 1 |
| Radiation type | Cu-$K_\alpha$ | Cu-$K_\alpha$ | Cu-$K_\alpha$ |
| Wavelength [Å] | 1.5418 | 1.5418 | 1.5418 |
| Temperature [K] | 293 | 293 | 293 |
| Data collection method | $\theta$-$2\theta$ scan | $\theta$-$2\theta$ scan | $\theta$-$2\theta$ scan |
| Increment in $2\theta$ [°] | 0.02 | 0.02 | 0.02 |
| $2\theta$ range [°] | 8–90 | 8–80 | 8–80 |
| Refinement on | – | $I_{net}$ | $I_{net}$ |
| $R_B$ | – | 0.047 | 0.040 |
| $R_{DDM}$ | – | 0.138 | 0.129 |
| H-atom treatment | – | H atoms constrained | H atoms constrained |
| Weighting scheme | – | based on measured s.u. values | based on measured s.u. values |
| CCDC- | – | 271215 | 271216 |

  

Table 2. Fractional atomic coordinates, occupancies and isotropic displacement parameters [Å$^2$] for **B**.

| | Occupancy | *x* | *y* | *z* | $B_{iso}$ |
|---|---|---|---|---|---|
| Fe(1) | 0.59(1) | 0 | 0 | 0 | 5.7(2) |
| N(1) | 0.59(1) | 0.1150(28) | 0.1812(26) | 0.1618(31) | 8.5(3) |
| N(2) | 0.59(1) | 0.2849(16) | 0.3786(17) | 0.2686(30) | 8.5(3) |
| C(1) | 0.59(1) | 0.2459(23) | 0.2819(30) | 0.1410(27) | 8.5(3) |
| C(2) | 0.59(1) | 0.1717(28) | 0.3405(27) | 0.3575(27) | 8.5(3) |
| C(3) | 0.59(1) | 0.0730(22) | 0.2132(30) | 0.3038(46) | 8.5(3) |
| C(4) | 0.59(1) | 0.4130(13) | 0.4992(14) | 0.3088(50) | 8.5(3) |
| B(1) | 0.50(3) | 2/3 | 1/3 | 0.2400(41) | 18.5(5) |
| F(1) | 0.50(3) | 2/3 | 1/3 | 0.0714(29) | 18.5(5) |
| F(2) | 0.50(3) | 0.7275(21) | 0.4631(17) | 0.3062(36) | 18.5(5) |
| Fe(1A) | 0.41 | 0 | 0 | 1/2 | 5.7 |
| N(1A) | 0.41 | 0.1150 | 0.1812 | 0.3382 | 8.5 |
| N(2A) | 0.41 | 0.2849 | 0.3786 | 0.2314 | 8.5 |
| C(1A) | 0.41 | 0.2459 | 0.2819 | 0.3590 | 8.5 |
| C(2A) | 0.41 | 0.1717 | 0.3405 | 0.1425 | 8.5 |
| C(3A) | 0.41 | 0.0730 | 0.2132 | 0.1962 | 8.5 |
| C(4A) | 0.41 | 0.4130 | 0.4992 | 0.1912 | 8.5 |
| B(1A) | 0.50 | 2/3 | 1/3 | 0.2600 | 18.5 |
| F(1A) | 0.50 | 2/3 | 1/3 | 0.4286 | 18.5 |
| F(2A) | 0.50 | 0.7275 | 0.4631 | 0.1938 | 18.5 |

Table 3. Fractional atomic coordinates, occupancies and isotropic displacement parameters (Å$^2$) for **C**.

| | Occupancy | *x* | *y* | *z* | $B_{iso}$ |
|---|---|---|---|---|---|
| Ni(1) | 0.58(1) | 0 | 0 | 0 | 5.2(1) |
| N(1) | 0.58(1) | 0.1051(21) | 0.1731(17) | 0.1594(20) | 9.4(2) |
| N(2) | 0.58(1) | 0.2793(10) | 0.3692(11) | 0.2558(31) | 9.4(2) |
| C(1) | 0.58(1) | 0.2353(18) | 0.2714(20) | 0.1291(20) | 9.4(2) |
| C(2) | 0.58(1) | 0.1734(20) | 0.3396(20) | 0.3620(17) | 9.4(2) |
| C(3) | 0.58(1) | 0.0712(18) | 0.2114(22) | 0.3016(30) | 9.4(2) |
| C(4) | 0.58(1) | 0.4071(9) | 0.4926(10) | 0.2960(24) | 9.4(2) |
| B(1) | 0.50(3) | 2/3 | 1/3 | 0.2550(44) | 16.8(4) |
| F(1) | 0.50(3) | 2/3 | 1/3 | 0.0837(26) | 16.8(4) |
| F(2) | 0.50(3) | 0.7260(12) | 0.4669(10) | 0.3166(19) | 16.8(4) |
| Ni(1A) | 0.42 | 0 | 0 | 1/2 | 5.2 |
| N(1A) | 0.42 | 0.10510 | 0.17310 | 0.34060 | 9.4 |
| N(2A) | 0.42 | 0.27930 | 0.36920 | 0.24420 | 9.4 |
| C(1A) | 0.42 | 0.23530 | 0.27140 | 0.37090 | 9.4 |
| C(2A) | 0.42 | 0.17340 | 0.33960 | 0.13800 | 9.4 |
| C(3A) | 0.42 | 0.07120 | 0.21140 | 0.19840 | 9.4 |
| C(4A) | 0.42 | 0.40710 | 0.49260 | 0.20400 | 9.4 |
| B(1A) | 0.50 | 2/3 | 1/3 | 0.24500 | 16.8 |
| F(1A) | 0.50 | 2/3 | 1/3 | 0.41630 | 16.8 |
| F(2A) | 0.50 | 0.72600 | 0.46690 | 0.18340 | 16.8 |

### Mössbauer Spectroscopy and DC Magnetic Measurements

Mössbauer studies performed at room temperature (Figure 4) exhibit a single asymmetric quadrupole doublet [½eqQ = 0.558(5)] with an isomer shift of *IS* = 1.065(5) mm/s and a line width of 0.27 mm/s.[15] This relatively high *IS* value is assigned to $Fe^{2+}$ in the high-spin state. The quadrupole splitting obtained is a result of the small distortion away from octahedral symmetry as discussed above. The narrow line width indicates clearly that, as far as the Fe ions are concerned, the measured sample is a single-phase material. The asymmetry in the doublet lines is due to a texture effect produced on the particles during the Mössbauer study.

Table 4. Selected geometric parameters [Å, °] for **B** and **C**.

| | | | |
|---|---|---|---|
| **B** | | | |
| Fe(1)–N(1) | 2.186(24) | N(1)–Fe(1)–N(1)[a] | 89.8(8) |
| N(1)–C(1) | 1.346(31) | Fe(1)–N(1)–C(1) | 127.2(20) |
| C(1)–N(2) | 1.373(34) | Fe(1)–N(1)–C(3) | 127.6(21) |
| N(2)–C(2) | 1.319(34) | N(1)–C(1)–N(2) | 111.3(23) |
| C(2)–C(3) | 1.368(34) | C(1)–N(2)–C(2) | 104.3(21) |
| C(3)–N(1) | 1.320(46) | N(2)–C(2)–C(3) | 109.1(25) |
| N(2)–C(4) | 1.436(19) | C(2)–C(3)–N(1) | 109.1(27) |
| B(1)–F(1) | 1.311(38) | C(3)–N(1)–C(1) | 105.2(26) |
| B(1)–F(2) | 1.367(22) | C(4)–N(2)–C(1) | 132.8(19) |
| | | C(4)–N(2)–C(2) | 122.9(20) |
| | | F(1)–B(1)–F(2) | 112.1(11) |
| | | F(2)–B(1)–F(2)[b] | 106.7(9) |
| **C** | | | |
| Ni(1)–N(1) | 2.091(15) | N(1)–Ni(1)–N(1)[a] | 91.4(5) |
| N(1)–C(1) | 1.334(23) | Ni(1)–N(1)–C(1) | 122.3(14) |
| C(1)–N(2) | 1.365(26) | Ni(1)–N(1)–C(3) | 132.9(14) |
| N(2)–C(2) | 1.340(26) | C(3)–N(1)–C(1) | 104.8(18) |
| C(2)–C(3) | 1.392(24) | N(1)–C(1)–N(2) | 109.9(16) |
| C(3)–N(1) | 1.306(31) | C(1)–N(2)–C(2) | 109.0(15) |
| N(2)–C(4) | 1.438(13) | N(2)–C(2)–C(3) | 102.5(17) |
| B(1)–F(1) | 1.329(40) | C(2)–C(3)–N(1) | 113.5(18) |
| B(1)–F(2) | 1.380(16) | C(4)–N(2)–C(1) | 135.3(13) |
| | | C(4)–N(2)–C(2) | 115.7(13) |
| | | F(1)–B(1)–F(2) | 110.3(6) |
| | | F(2)–B(1)–F(2)[b] | 108.6(5) |

[a] *y*, *x* + *y*, –*z*. [b] 1 – *y*, *x* – *y*, *z*.

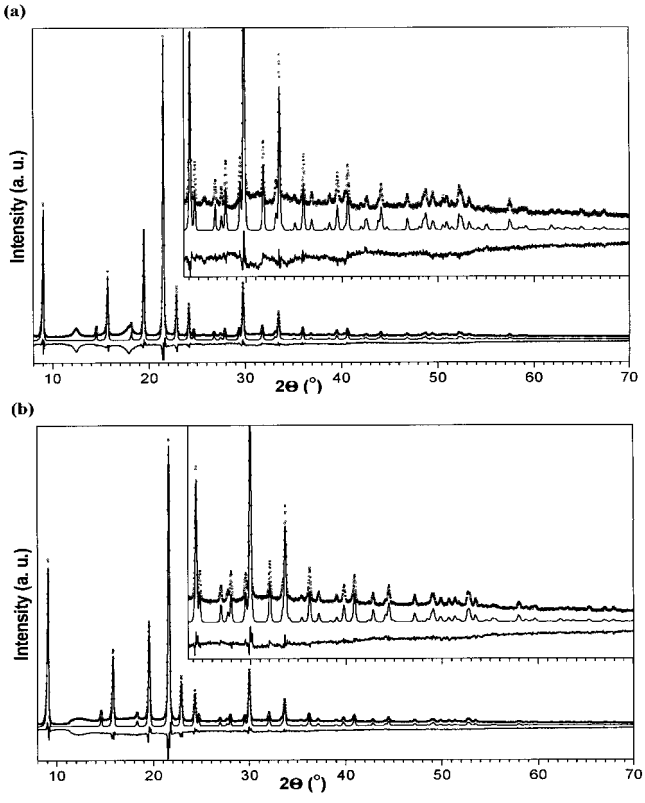


Figure 1. Observed (circles), calculated (solid line), and difference (bottom curve) PXRD profiles for **B** (a) and **C** (b) after the DDM structure refinement.

  

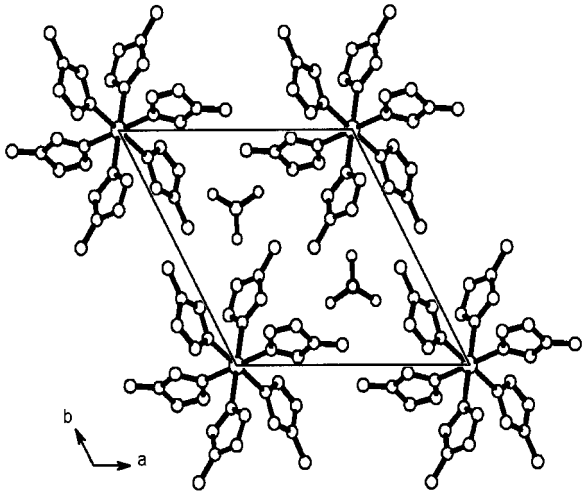


Figure 2. Projection *ab* of the crystal structure of **B** and **C**.

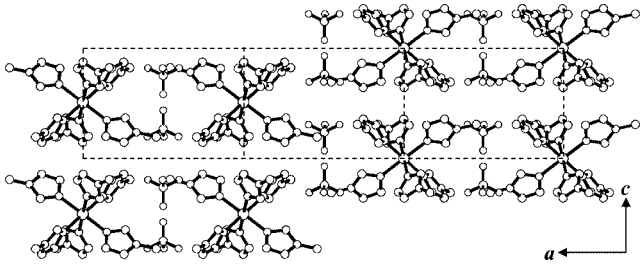


Figure 3. Alternative positions of molecules in the crystals of **B** and **C**. The unit cell boundaries are shown by dashed lines.

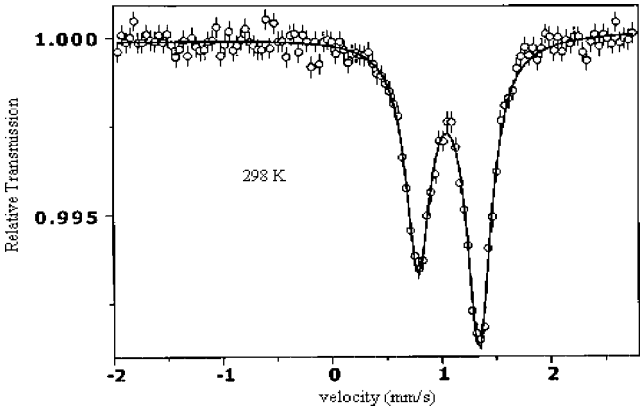


Figure 4. $^{57}$Fe Mössbauer spectrum of $(C_4H_6N_2)_6Fe(BF_4)_2$ measured at 298 K.

In order to depict the high-spin state of $Fe^{2+}$ ions in (1-methylimidazole)$_6$Fe(BF$_4$)$_2$, DC magnetic measurements were performed. DC magnetic measurements shown in Figure 5 conclusively confirm the high-spin state of $Fe^{2+}$, which is similar to the reports of high-spin $Fe^{2+}$ compounds containing imidazole derivatives as ligands.[16a–16c] The temperature dependence of the susceptibility (measured at 1 T) have the typical paramagnetic shape down to 5 K, and adheres to the Curie–Weiss law: $\chi(T) = \chi_0 + C/(T - \theta)$, where $\chi_0$ is the temperature-independent part of $\chi$, $C$ is the Curie constant, and $\theta$ is the Curie–Weiss temperature. The fit (solid line) yields: $\chi_0$ = –0.0008 emu/mol Oe, $C$ = 4.21(2) emu K/mol Oe and $\theta$ = –3.8(1) K. The linear isothermal magnetization (up to 1 T) shown in the inset confirms the paramagnetic nature at 5 K. The extracted paramagnetic effective moment is $P_{eff}$ = 5.78 $\mu_B$, a value which is midway between the common experimental 5.4 $\mu_B$ and the free ion $P_{eff}$ = 6.7 $\mu_B$ (no spin-orbit coupling) for the high-spin state of $Fe^{2+}$ ions.[17,18]

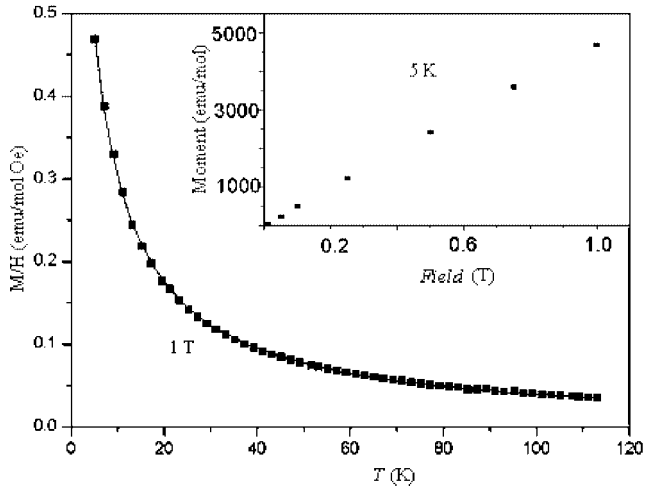


Figure 5. The DC magnetic susceptibility of $(C_4H_6N_2)_6Fe(BF_4)_2$ and linear $M(H)$ curve at 5 K.

## Magnetic Measurements

The (imidazole)metal complexes show paramagnetic behavior[18,19] which can be seen in Figure 6. Higher magnetization values are measured for the (imidazole)iron complexes as compared to the (imidazole)nickel complexes, due to the different electronic ground-state configurations of the

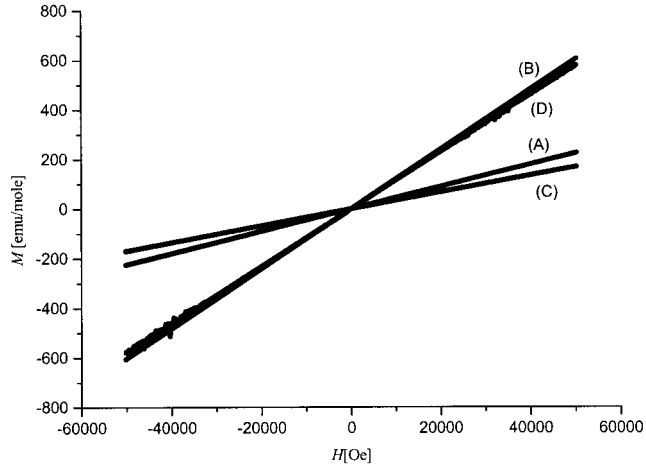


Figure 6. Comparison studies of the magnetization curve at room temperature for $(C_4H_6N_2)_6Ni(PF_6)_2$ (**A**), $(C_4H_6N_2)_6Fe(BF_4)$ (**B**)$_2$, $(C_4H_6N_2)_6Ni(BF_4)_2$ (**C**), and $(C_4H_6N_2)_6Fe(PF_6)$ (**D**).[6]

  

$Fe^{2+}(d^6)$ and $Ni^{2+}(d^8)$ ions in the complexes, with the theoretical spin magnetic moment ($\mu_s$) values being $d^6$ = 4.90 B.M. and $d^8$ = 2.83 B.M., respectively. The (imidazole)-iron complexes shows similar magnetization properties whereas the (imidazole)nickel complexes are different. The change in magnetization can be observed due to interference of the orbital motion of the electron with the electric fields of the other atoms, ions, and molecules surrounding the metal ions.[20] The magnetizations of the synthesized (imidazole)metal complexes do not saturate in the range of the applied magnetic field.

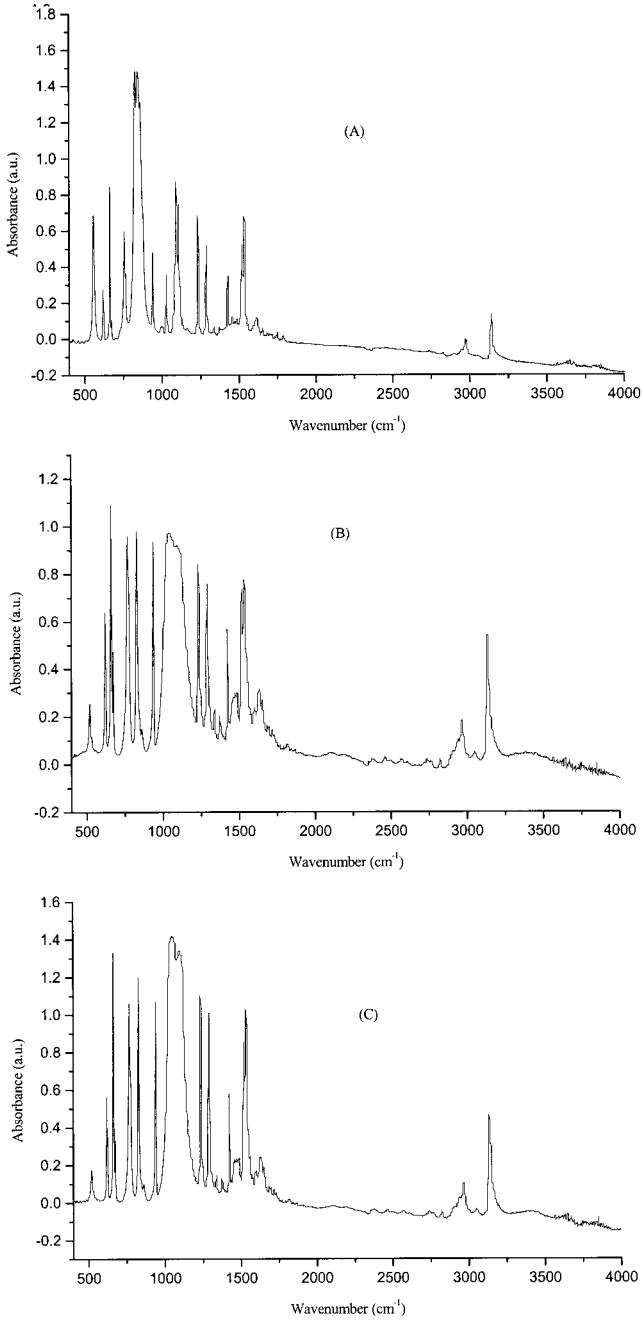


Figure 7. IR absorption spectra of the complexes $(C_4H_6N_2)_6Ni(PF_6)_2$ (**A**), $(C_4H_6N_2)_6Fe(BF_4)_2$ (**B**), and $(C_4H_6N_2)_6Ni(BF_4)_2$ (**C**).

### Infrared and Raman Spectroscopy

The IR and Raman spectra are recorded for the iron and nickel complexes. They provide support to the characterization of the product by identifying the vibration of the ligands surrounding the central transition metal ion. The IR absorption spectra for the $(C_4H_6N_2)_6Ni(PF_6)_2$ (**A**), $(C_4H_6N_2)_6Fe(BF_4)_2$ (**B**) and $(C_4H_6N_2)_6Ni(BF_4)_2$ (**C**) are illustrated in Figure 7 (a, b, c). Table 5 shows the comparisons of the proposed assignments with those reported in the literature for the bands observed in the complexes of iron (**B**) and nickel (**A** and **C**).[18,19] The vibrational bands assigned to the organic ligand, $C_4H_6N_2$, are mostly blue-shifted, but some are assigned as shifted to the red. Our conclusion is that on average, the assigned bands illustrated in Table 5 are in good agreement with the interpretation of Reedijk,[18,19] Perchard and Novak.[20] The M–N vibrations are observed in the Raman spectra below 300 $cm^{-1}$ and their locations agree with the literature values.[18,19] The IR and Raman active vibrations due to $BF_4^-$ and $PF_6^-$ anions are present in the spectra and also match the literature values.[21,22] Smaller shifts are observed for these bands, as compared with the literature values. The intense Raman line for the $PF_6^-$ ion assigned to the symmetric mode $\nu_1$ = 742 $cm^{-1}$ is present in the $(C_4H_6N_2)_6Ni(PF_6)_2$ (**A**) spectra.[22] The IR and Raman active vibrations due to the $BF_4^-$ ion for the $(C_4H_6N_2)_6Fe(BF_4)_2$ (**B**) and $(C_4H_6N_2)_6Ni(BF_4)_2$ (**C**) complexes are shown in Table 6. The Raman and IR measurements strengthen our assignment of the ligands surrounding the Fe and Ni ions. The observed vibration bands for the $PF_6^-$ and $BF_4^-$ anions confirm that the anions are not bonded to the metal ions.[19,23]

### NMR Spectroscopy

$^1H$ and $^{13}C$ NMR signals are probably too broad to be observed due to the paramagnetic properties of the iron and nickel complexes. The $^{19}F$ NMR spectrum [Figure 8 (a)] confirms the presence of $PF_6^-$ in the $(C_4H_6N_2)_6Ni(PF_6)_2$ complex (**A**). The $^{19}F$ NMR spectra of $(C_4H_6N_2)_6Fe(BF_4)_2$ (**B**) and $(C_4H_6N_2)_6Ni(BF_4)_2$ (**C**) are presented in Figure 8 (b, c). The observed singlets (the coupling constant to boron is known to be very small in this anion[24]) have a shoulder deriving from the minor $^{10}B$ isotopomer (the isotope effect is 54 ppb). The NMR spectroscopic results reveal relatively narrow $^{19}F$ peaks. Thus, this demonstrates that the $PF_6^-$ and $BF_4^-$ anions are not bonded to the metal cations; see for instance ref.[25]

### EPR Spectroscopy

The continuous wave electron paramagnetic resonance (cwEPR) spectroscopy is used to probe the point symmetry of the nickel complexes.

The EPR powder spectrum of (1-methylimidazole)$_6$-$Ni(PF_6)_2$ (**A**) and (1-methylimidazole)$_6Ni(BF_4)_2$ (**C**) at 3425G are presented in Figure 9 (a, b). These complexes

  

Table 5. IR and Raman vibrational bands [$cm^{-1}$] for the complexes $(C_4H_6N_2)_6Ni(PF_6)_2$ (**A**), $(C_4H_6N_2)_6Fe(BF_4)_2$ (**B**), and $(C_4H_6N_2)_6Ni(BF_4)_2$ (**C**).

| Liquid ligand | | | Vibration frequency | | | | | |
|---|---|---|---|---|---|---|---|---|
| | | | $(C_4H_6N_2)_6Ni(PF_6)_2$ (**A**) | | $(C_4H_6N_2)_6Fe(BF_4)_2$ (**B**) | | $(C_4H_6N_2)_6Ni(BF_4)_2$ (**C**) | |
| IR | Raman | Assignment | IR | Raman | IR | Raman | IR | Raman |
| 3131 w | 3128 | C–H stretching | 3139 m | 3158 s | 3134 s | 3155 s | 3133 s | 3160 s |
| 3105 m | 3103 | C–H stretching | – | – | – | – | – | – |
| 3009 sh | 3000 | | – | – | – | – | – | – |
| 2986 sh | 2951 | $CH_3$ stretchings | 2972 m | 2973 s,b | 2966 m,b | 2968 s,b | 2965 m | 2966 s |
| 2952 m | | | 2949 sh | 2823 w | 2942 sh | 2823 w | 2941 sh | 2822 w |
| 1675 w | | combination bands | 1652 w | – | 1651 w | – | 1651 w | – |
| 1589 w | | | 1610 w | | 1632 w | | 1620 w | |
| 1518 s | 1510 | ring stretching ($R_1$) | 1533 s | 1532 s | 1532 s | 1516 s | 1532 s | 1517 s |
| 1506 sh | 1500 | ring stretching ($R_2$) | 1518 sh | | 1515 sh | | 1518 sh | |
| 1463 w | 1472 | $CH_3$ bending | 1487–1455 w | – | 1485–1456 w | – | 1486–1465 w | – |
| 1421 m | 1420 | $CH_3$ bending | 1425 s | 1423 s | 1421 s | 1421 s | 1421 s | 1421 s |
| 1361 w | 1353 | ring stretching ($R_3$) | 1373 w | 1350 s,b | 1372 w | 1350 s | 1373 w | |
| 1328 w | 1328 | ring stretching ($R_4$) | 1337 w | | 1336 w | | 1338 w | 1338 s,b |
| 1286 s | 1288 | in-plane C–H bending | 1288 s | 1287 s | 1288 s | 1288 s | 1289 s | 1289 s,b |
| 1232 vs | 1230 | ring stretching ($R_5$) + CN stretching | 1234 s | 1232 w | 1233 s | 1233 w | 1234 s | 1234 w |
| 1109 s | 1105 | in-plane C–H bending | 1109 s | | 1100 s | | 1111 s,b | |
| 1078 vs | 1075 | in-plane C–H bending | 1092 s | 1092 sb | 1092 s,b | 1095 s,b | 1096 s,b | 1097 s,b |
| 1029 m | 1025 | $CH_3$ deformation | 1028 m | 1027 s | 1036 | 1028 s | 1037 s,b | 1028 s |
| 909 s | 904 | ring stretching ($R_6$) | 939 s | 938 w | 936 s | 936 s | 939 s | 938 w |
| 860 sh | 847 | out-of-plane C–H bending | 859 s,b | 851 w | 860 sh | 858 w | 860 sh | 857 w |
| 821 s | 818 | out-of-plane C–H bending | 826 s,b | – | 827 s | – | 827 s | – |
| 744 s | 740 | out-of-plane C–H bending | 764 sh, 756 s | 742 s | 767 s | 769 s,b | 774 sh, 766 s | 763 s |
| 665 vs | 665 | ring stretching and CN stretching | 673 sh, 663 s | 670 s | 673 sh, 660 s | 670 s | 674 sh, 662 s | 671 s |
| 618 s | 616 | ring deformation | 618 m | – | 619 s | – | 619 s | – |
| 355 w | 353 | C–N deformation | – | 375 s | – | 371 s | – | 376 s |
| 224 w | 220 | C–N deformation | – | 246 s | – | 236 s | – | 247 s |

Table 6. IR and Raman active vibtational bands of the $BF_4^-$ anion in $(C_4H_6N_2)_6Fe(BF_4)_2$ (**B**) and $(C_4H_6N_2)_6Ni(BF_4)_2$ (**C**).

| $[BF_4^-]$ | $Fe(C_4H_6N_2)_6(BF_4)_2$ (**B**) | | | | $Ni(C_4H_6N_2)_6(BF_4)_2$ (**C**) | | | |
|---|---|---|---|---|---|---|---|---|
| | $\nu_1$ | $\nu_2$ | $\nu_3$ | $\nu_4$ | $\nu_1$ | $\nu_2$ | $\nu_3$ | $\nu_4$ |
| IR [$cm^{-1}$] | 662–664 | – | 1037–1111 | 519–532 | 660–673 | – | 1036–1092 | 519–532 |
| Raman [$cm^{-1}$] | 769 | 371 | 1028 | 520 | 763 | 376 | 1028 | 520 |

contain $Ni^{2+}$ with $3d^8$ in octahedral symmetry, where the ground-term $^3A_{2g}$ nondegenerate state arises from the $(t_{2g})^6(e_g)^2$ configuration. Distortions from perfect octahedral symmetry result in a zero-field splitting of the three $S = 1A_{2g}$ terms ($m_s = 1$, 0, or –1). Transitional metal systems with $S = 1$ are often "EPR-silent" in the x-band EPR because of large zero-field splitting. The existence of an EPR spectrum Figure 9 (a, b) indicates a high symmetry about the metal atom, with a small zero-field splitting (less than the applied frequency, i.e. 9.7 GHz). The zero-field splitting arises from lowering, to some extent, the point symmetry from $O_h$, causing unequal magnetic field splitting, $m_s(-1) \leftrightarrow m_s(0)$ and $m_s(0) \leftrightarrow m_s(+1)$ transitions of the $^3A_{2g}$ ground state admixture with components of the nearest excited state, $^3T_{2g}$ [arises from the $(t_{2g})^5(e_g)^3$ configuration $^3T_{2g}$ state]. It is noticable that the two spectrum lines are very broad, which is commonly observed in concentrated paramagnetic samples.[9] Comparing the cwEPR spectrum of (1-methylimidazole)$_6$Ni$(PF_6)_2$ (**A**) with that of (1-methylimidazole)$_6$Ni$(BF_4)_2$ (**C**), we found that complex **C** shows more crystalline properties as complex **A**. The cwEPR spectra of the nickel complexes are consistent with powder spin-triplet systems reported in the literature.[9,18,19]

## Thermal Analysis

To probe the mechanism of the reaction, we had to learn more about the thermal stability of the synthesized complexes, the precursors, and the ionic liquids. This was reached by studying the thermogravimetry analysis (TGA) of the products and the ionic liquids between 25 and 1000 °C with a heating rate of 3 °C $min^{-1}$ under an $N_2$ flow. The TGA curve is shown in Figure 10 (a) for the $(C_4H_6N_2)_6Ni(PF_6)_2$ (**A**), $(C_4H_6N_2)_6Fe(BF_4)_2$ (**B**), $(C_4H_6N_2)_6Ni(BF_4)_2$ (**C**) and $(C_4H_6N_2)_6Fe(PF_6)_2$ (**D**) complexes. The TGA curve reveals that the anions affect the stability of the complexes.[26,27] The weight loss measured at a temperature of 250 °C, determined from the curve in Figure 10 (a), is 6.74% (0.28 mg) for **A**, 2.00% (0.11 mg) for **B**, 5.38% (0.23 mg) for **C** and 27.25% (1.01 mg) for **D**. The TGA curve shows that the $BF_4^-$ anion complexes are more stable

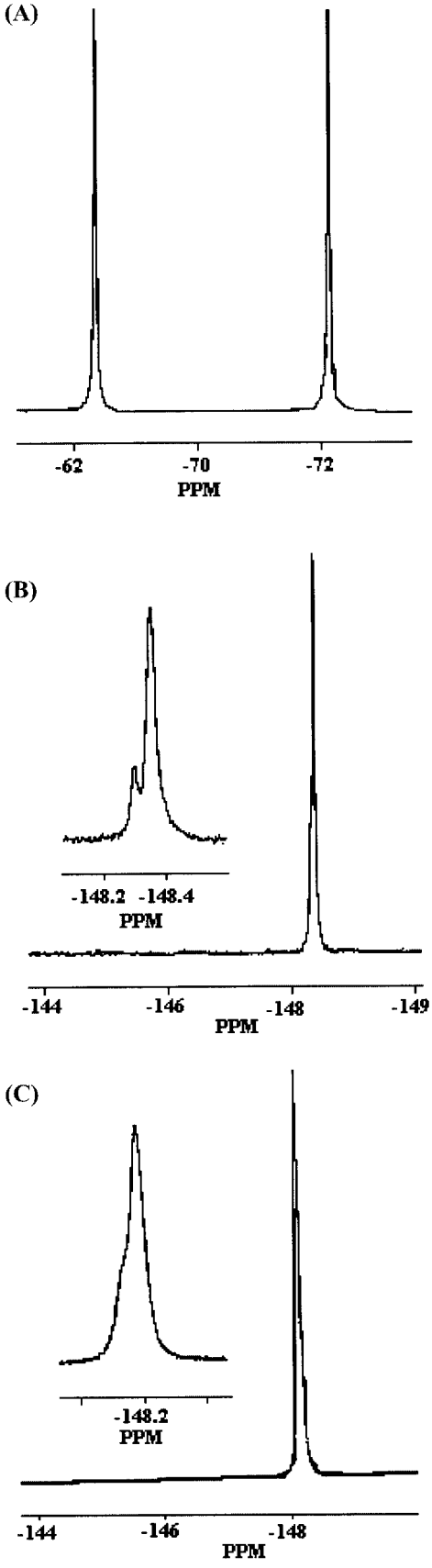


Figure 8. $^{19}F$ NMR spectra for $(C_4H_6N_2)_6Ni(PF_6)_2$ (**A**), $(C_4H_6N_2)_6Fe(BF_4)_2$ (**B**), and $(C_4H_6N_2)_6Ni(BF_4)_2$ (**C**).

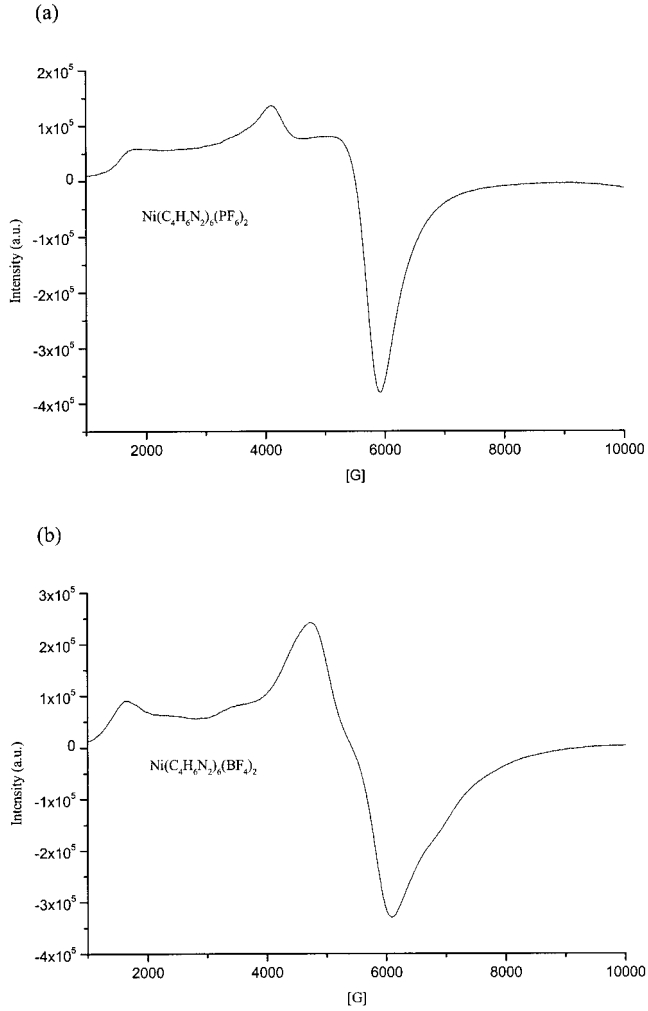


Figure 9. X-band EPR spectra of $Ni^{2+}$ powder complexes at room temperature of $(C_4H_6N_2)_6Ni(PF_6)_2$ (a), and $(C_4H_6N_2)_6Ni(BF_4)_2$ (b).

than the $PF_6^-$ anion complexes for both iron and nickel. The thermal stability of the ionic[28] liquids employed in our reactions, $(BMI^+)(PF_6^-)$ and $(BMI^+)(BF_4^-)$, were also studied using TGA between 25 and 1000 °C at a flow rate of 3 °C min$^{-1}$ under $N_2$. The TGA graph of the ionic liquids is shown in Figure 10 (b), and the physical properties of the ionic liquid used for our reaction are summarized in Table 7. From Figure 10 (b) we observe at a temperature of 150 °C that there is no weight loss for the $(BMI^+)(PF_6^-)$ and $(BMI^+)(BF_4^-)$ ionic liquids. The decomposition temperature ranges of ionic liquids measured from TGA curves are found to be 332–516 °C $(BMI^+)(PF_6^-)$ and 309–528 °C $(BMI^+)(BF_4^-)$. The TGA curve confirms that the ionic liquids $(BMI^+)(PF_6^-)$ and $(BMI^+)(BF_4^-)$ are stable at the reaction temperature. They do not form a metal fluoride, or undergo any other decomposition at the reaction temperature.[29] It is therefore concluded from the TGA results that the ionic liquids react only as a result of the bubble's collapse.

  

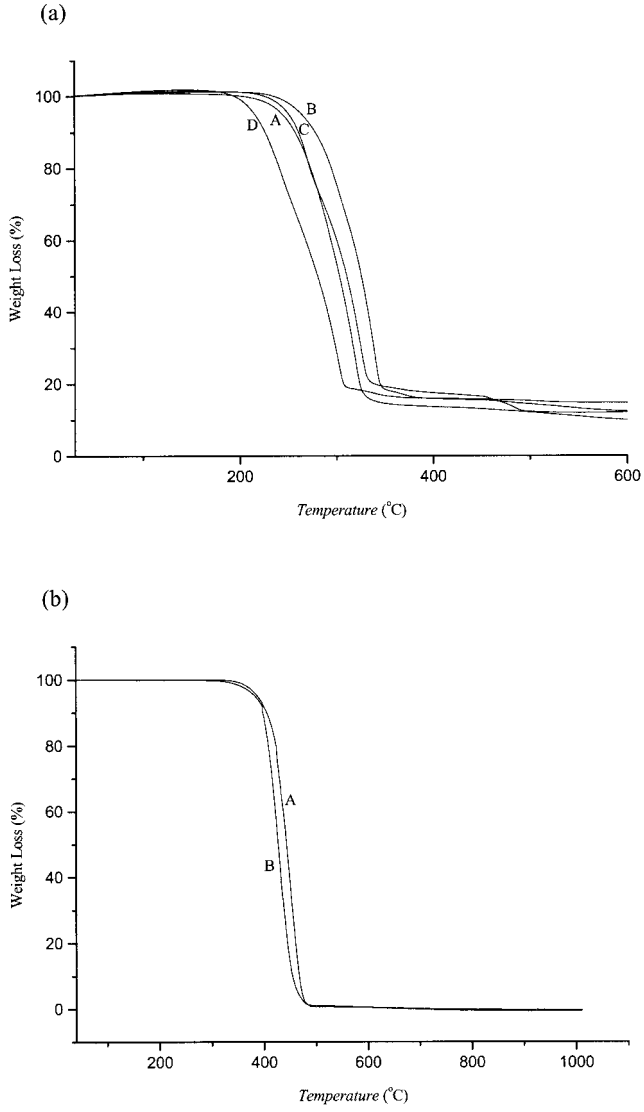


Figure 10. TGA curve (a) of iron and nickel complexes $(C_4H_6N_2)_6Ni(PF_6)_2$ (**A**), $(C_4H_6N_2)_6Fe(BF_4)_2$ (**B**), $(C_4H_6N_2)_6Ni(BF_4)_2$ (**C**), and $(C_4H_6N_2)_6Fe(PF_6)$ (**D**);[6] (b) TGA curve of ionic liquids (A) $(BMI)^+(PF_6)^-$ and (B) $(BMI)^+(BF_4)^-$.

## Conclusions

The synthesis of transition metal complexes in ionic liquids under ultrasonic conditions has given a new direction to the chemistry of ionic liquids. In brief, the sonication products of 1-methylimidazole and carbonylmetal complexes in ionic liquids $(BMI^+)(PF_6^-)$ and $(BMI^+)(BF_4^-)$ (which act as solvents) form the complexes $(C_4H_6N_2)_6Fe(PF_6)_2$,[6] $(C_4H_6N_2)_6Ni(PF_6)_2$, $(C_4H_6N_2)_6Fe(BF_4)_2$, and $(C_4H_6N_2)_6Ni(BF_4)_2$ when sonicated in air. The interesting part of this reaction under ultrasound conditions is that there is no hydrolysis of $PF_6$ in the presence of metals, and there are no reports of metathesis or decomposition of cations to give different products. In these reactions the anions of the ionic liquids contribute to the final structure of the products, as was stated in our previous paper[6] and in ref.[30] The sonochemical products of $Fe^{2+}$ and $Ni^{2+}$ ions are octahedrally coordinated by six 1-methylimidazole molecules. The $PF_6^-$ and $BF_4^-$ anions act as charge-stabilizing agents in the formation of the crystals, which are characterized by the trigonal lattice with the $P\bar{3}$ space group. The PXRD structure analysis revealed a high concentration of twin and/or line defects in the crystals. Thus, ionic liquid solvents are effective as donors of anions for the cation stabilization under ultrasonic conditions. Although a tremendous amount of work has been carried out on applications of ionic liquids, there have been a few reports in recent years where ionic liquids are used in sonochemistry. In particular, much work is still needed to explore and utilize the fundamental chemistry and properties of these interesting liquids in sonochemistry.

## Experimental Section

**General:** 1-Butyl-3-methylimidazolium hexafluorophosphate $(BMI^+)(PF_6^-)$ (96%), 1-butyl-3-methylimidazolium tetrafluoroborate $(BMI^+)(BF_4^-)$ (97%) and 1-methylimidazole were purchased from Aldrich. Pentacarbonyliron (99.5%) and tetracarbonylnickel (100%) were purchased from Strem Chemicals, USA; they were handled very carefully with safety precautions in an effective fume hood; refer to Material Safety Data Sheet (MSDS) for further information and safety measurements. PXRD data were collected with a Bragg–Brentano geometry using a DRON-4 diffractometer with a graphite secondary monochromator (Cu-$K_\alpha$ radiation, $\lambda$ = 1.5418 Å) and a scintillation counter. The measurements were carried out at room temperature under air. A $^{57}Fe$ Mössbauer study of (1-methylimidazole)$_6Fe(BF_4)_2$ was performed at ambient temperature using a conventional constant acceleration drive and a 50 mCi $^{57}Co$:Rh source. The experimental spectrum was analyzed by a least-squares fitting procedure, and the $^{57}Fe$ isomer shifts are relative to α-Fe, measured at room temperature. DC magnetic measurements were performed using a commercial (Quantum Design) super-conducting quantum interference device (SQUID) magnetometer. The magnetic measurements were performed with a Quantum Design MPMSXL SQUID magnetometer for $(C_4H_6N_2)_6Ni(PF_6)_2$ (**A**), $(C_4H_6N_2)_6Fe(BF_4)_2$ (**B**), $(C_4H_6N_2)_6Ni(BF_4)_2$ (**C**), and $(C_4H_6N_2)_6Fe(PF_6)_2$ (**D**). The magnetization was measured at room temperature as a function of an external field being swept up from –50 kOe to 50 kOe and down to –50 kOe in steps of 200 Oe. The IR absorption spectra of the complexes were recorded in the range of 400–4000 $cm^{-1}$ by means of a Nicolet (Impact 410) spectrometer with KBr pellets (5 mg of sample in 500 mg of KBr). Raman spectroscopic measurements were carried out at room temperature with a Jobin Yvon Horiba Raman system. The 524 nm line of an $Ar^+$ laser was used as the excitation source. The Raman spectra were recorded in the range 100–4000 $cm^{-1}$. Powder samples

Table 7. Physical properties of the ionic liquids.

| Ionic liquid | Decomposition temperature range (TGA) | Molecular weight [g/mol] | Density [g/ml] |
|---|---|---|---|
| 1-Butyl-3-methylimidazolium hexafluorophoshate (96%) | 332–516 °C | 284.18 | 1.510 |
| 1-Butyl-3-methylimidazolium tetrafluoroborate (97%) | 309–528 °C | 226.02 | 1.320 |

  

were measured at room temperature with a Bruker EPR 100d X-band spectrometer, frequency 9.766 GHz, microwave power 6.34 mW.

**Synthesis of the Complexes:** The synthetic procedure for the metal complexes of 1-metylimidazole in an ionic liquid under ultrasonic conditions is reported in our previous communication.[6] All the metal complexes of 1-methylimidazole were crystallized from ethanol (due to high solute solubility).[31]

**(1-Methylimidazole)$_6$Ni$^{II}$(PF$_6$)$_2$ (A):** $Ni(CO)_4$ (6.18 mmol, 1.056 g) and 1-methylimidazole (24 mmol, 2 g) were dispersed in ionic liquid ($BMI^+$)($PF_6^-$) (17.6 mmol, 5 g) under ultrasonic conditions. Transparent blue needle-shaped crystals (1.35 mmol, 1.141g) were obtained. $C_{24}H_{36}F_{12}N_{12}NiP_2$ (841.27): calcd. C 34.26, H 4.28, N 19.98; found C 34.70, H 4.47, N 19.73. $^{19}F$ NMR (188.3 MHz in [D$_6$]DMSO): δ = –70.25 (d, $J_{PF}$ = 709 Hz) ppm (confirming the presence of $PF_6^-$). MS (DCI, FAB): *m*/*z* = 82 [$C_4H_6N_2$], 145 [$PF_6$].

**(1-Methylimidazole)$_6$Fe$^{II}$(BF$_4$)$_2$ (B):** $Fe(CO)_5$ (6.08 mmol, 1.192 g) and 1-methylimidazole (24 mmol, 2 g) were dispersed in ionic liquid ($BMI^+$)($BF_4^-$) (22 mmol, 5 g) under ultrasonic conditions. Transparent needle-shaped crystals (2.16 mmol, 1.560g) were obtained. $C_{24}H_{36}B_2F_8FeN_{12}$ (722.09): calcd. C 39.88, H 4.98, N 23.26; found C 40.33, H 5.39, N 23.69. $^{19}F$ NMR (188.3 MHz in [D$_6$]-DMSO): δ = –148.35 ppm (confirming the presence of $BF_4^-$). MS (DCI, FAB): *m*/*z* = 82 [$C_4H_6N_2$], 87 [$BF_4$].

**(1-Methylimidazole)$_6$Ni$^{II}$(BF$_4$)$_2$ (C):** $Ni(CO)_4$ (6.18 mmol, 1.056 g) and 1-methylimidazole (24 mmol, 2 g) were dispersed in ionic liquid ($BMI^+$)($BF_4^-$) (22 mmol, 5 g) under ultrasonic conditions. Transparent blue needle-shaped crystals (1.41 mmol, 1.024g) were obtained. $C_{24}H_{36}B_2F_8N_{12}Ni$ (724.95): calcd. C 39.72, H 4.96, N 23.17; found C 40.44, H 5.35, N 23.31. $^{19}F$ NMR (188.3 MHz in [D$_6$]DMSO): δ = –148.19 ppm (confirming the presence of $BF_4^-$). MS (DCI, FAB): *m*/*z* = 82 [$C_4H_6N_2$], 87 [$BF_4$].


[1] a) T. Welton, *Chem. Rev.* **1999**, *99*, 2071–2083; b) J. Dupont, R. Souza, P. Suarez, *Chem. Rev.* **2002**, *102*, 3667–3692; c) D. Zhao, M. Wu, Y. Kon, E. Min, *Catal. Today* **2002**, *74*, 157–189; d) K. Marsh, A. Deev, A. Wu, E. Tran, A. Klamt, *Korean J. Chem. Eng.* **2002**, *19*, 357–362.

[2] L. Xu, W. Chen, J. Xiao, *Organometallics* **2000**, *19*, 1123–1127.

[3] C. Mathews, P. Smith, T. Welton, A. White, D. Williams, *Organometallics* **2001**, *20*, 3848–3850.

[4] S. Christie, S. Subramanian, L. Wang, M. J. Zaworotko, *Inorg. Chem.* **1993**, *32*, 5415–5417.

[5] K. Jin, X. Huang, L. Pang, J. Li, A. Appel, S. Wherland, *Chem. Commun.* **2002**, 2872–2873.

[6] D. Jacob, V. Kahlenberg, K. Wurst, L. A. Solovyov, I. Felner, L. Shimon, H. Gottlieb, A. Gedanken, *Eur. J. Inorg. Chem.* **2005**, 522–528.

[7] a) K. S. Suslick, S. B. Choe, A. A. Cichowlas, M. W. Grinstaff, *Nature* **1991**, *353*, 414–416; b) Y. Koltypin, G. Kataby, X. Cao, R. Prozorov, A. Gedanken, *J. Non-Cryst. Solids* **1996**, *201*, 159–162.

[8] K. V. P. M. Shafi, Y. Koltypin, A. Gedanken, R. Prozorov, J. Balogh, J. Lendvai, I. Felner, *J. Phys. Chem. B* **1997**, *101*, 6409–6414.

[9] D. Collison, M. Helliwell, V. M. Jones, F. E. Mabbs, E. J. L. McInnes, P. C. Riedi, G. M. Smith, R. G. Pritchard, W. I. Cross, *J. Chem. Soc., Faraday Trans.* **1998**, *94*, 3019–3025.

[10] E. J. Van den Heuvel, P. L. Franke, G. C. Verschoor, A. P. Zuur, *Acta Crystallogr. C* **1983**, *39*, 337–339.

[11] L. A. Solovyov, *J. Appl. Crystallogr.* **2004**, *37*, 743–749.

[12] H. M. Rietveld, *J. Appl. Crystallogr.* **1969**, *2*, 65–71.

[13] D. B. Wiles, R. A. Young, *J. Appl. Crystallogr.* **1981**, *14*, 149–151.

[14] a) I. R. Baird, S. J. Rettig, B. R. James, K. A. Skov, *Can. J. Chem.* **1998**, *76*, 1379–1388; b) E. J. Heuvel, P. L. Franke, G. C. Verschoor, A. P. Zuur, *Acta Crystallogr. C* **1983**, *39*, 337–339.

[15] B. L. Little, G. J. Long, *Inorg. Chem.* **1978**, *17*, 3401–3413.

[16] a) G. Carver, P. L. W. Tregenna-Piggott, A. Barra, A. Neels, J. A. Stride, *Inorg. Chem.* **2003**, *42*, 5771–5777; b) J. A. Garcia'-Va'zquez, J. Romero, A. Sousa-Pedrares, A. Sousa, A. D. Garnovskii, D. A. Garnovskii, *J. Chem. Crystallogr.* **2000**, *30*, 23–26; c) F. Seel, R. Lehnert, E. Bill, A. Trautwein, *Z. Naturforsch. B: Anorg.Chem., Org. Chem.* **1980**, *35B*, 631–638.

[17] M. M. Schieber, *Experimental Magnetochemistry*, North Holland Publishers, Amsterdam, **1967**, p. 23.

[18] J. Reedijk, *Inorg. Chim. Acta* **1969**, *3*, 517–522.

[19] J. Reedijk, *J. Inorg. Nucl. Chem.* **1971**, *33*, 179–188.

[20] F. A. Cotton, G. Wilkinson, *Advanced Inorganic Chemistry*, John Wiley & Sons, Inc., New York, **1962**, pp. 505–508.

[21] C. Perchard, A. Novak, *Spectrochim. Acta* **1967**, *23A*, 1953.

[22] N. Greenwood, *J. Chem. Soc.* **1959**, 3811–3815.

[23] K. Nakamoto, *Infrared Spectra of Inorganic and Coordination Compounds*, Wiley, New York, **1963**.

[24] L. Woodward, L. Anderson, *J. Inorg. Nucl. Chem.* **1956**, *3*, 326–327.

[25] H. Günther, *NMR Spectroscopy*, John Wiley & Sons, Chichester, **1980**, p. 220.

[26] K. Kuhlmann, D. M. Grant, *J. Phys. Chem.* **1964**, *68*, 3208–3213.

[27] J. Dam, G. Hakvoort, J. Jansen, J. Reedijk, *J. Inorg. Nucl. Chem.* **1975**, *37*, 713–718.

[28] a) K. J. Baranyai, G. B. Deacon, D. R. MacFarlane, J. M. Pringle, J. L. Scott, *Aust. J. Chem.* **2004**, *57*, 145–147; b) M. Kosmulski, J. Gustafsson, J. B. Rosenholm, *Thermochim. Acta* **2004**, *412*, 47–53.

[29] G. S. Fonseca, A. P. Umpierre, P. F. P. Fichtner, S. R. Teixeira, J. Dupont, *Chem. Eur. J.* **2003**, *9*, 3263–3269.

[30] K. Jin, X. Huang, L. Pang, J. Li, A. Appel, S. Wherland, *Chem. Commun.* **2002**, 2872–2873.

[31] B. Pamplin, *Crystal Growth*, Pergamon Press, Oxford, **1980**, vol. 16, pp. 395–420.


Received: January 10, 2005
Published Online: May 27, 2005

  